[1] Linhao Wang*

Topologies and Control Strategies for High-performance Power Electronic Converters

Journal of Electrical Systems

Abstract: - Distribution networks require power electronic converters that can have a fast enough response time and at the same time be able to operate stably. In this paper, a dual Boost PFC topology is used to achieve high power density and performance by connecting Boost PFC converters in parallel. SCR and switching are utilized for precise control to reduce harmonic pollution and improve power supply stability to meet the demands of precision equipment. The CCM control method, combined with direct duty cycle calculation, is used to realize efficient and intelligent control of the Boost PFC converter. The method eliminates the need for current sampling, reduces cost, and improves control speed and DSP resource utilization. The stability of the output voltage and the fast response to load changes are ensured by the precise design of the voltage control loop. The PSIM software is utilized to build a simulation circuit with 220V single-phase AC input, DC output voltage of 336V, and output power of 3.6kW with a fixed power load. Under different working conditions, the input current can track the input voltage well, and the output voltage is stable.The CCM control strategy shows the fastest regulation speed and the best voltage stability when the voltage reference value increases suddenly, the regulation time is only 30ms, and the voltage change is only 1V. Under the input voltage of 200V, the efficiency of the circuit is high at medium load, and there is room for improvement at light load and high load. Comparison with MPPT and MPC-MPPT strategies shows significant advantages.

Keywords: electronic converter; Boost PFC topology; voltage control; resource utilization; CCM control strategy

1. INTRODUCTION

Power transformers have a hundred years of development history, and are widely used in power systems with mature development in performance [1]. However, with the development of smart grid and energy Internet and other technologies, only with the voltage conversion, electrical isolation and other functions can not meet the requirements of the smart grid, its own no-load loss, waveform distortion and other problems are prominent [2]. Nowadays, power semiconductor devices continue to develop and power electronics technology is mature, so power electronic transformers are widely studied [3-4]. The outstanding advantages of power electronic transformers, also known as smart transformers, are small size, light weight, the ability to manage harmonics, reactive power compensation on the AC side, controllable original square current, fault isolation between ports, and direct access to distributed power supplies [5-7]. Power electronic transformers are widely used in electric locomotive traction system, new energy DC grid connection, smart grid and electric vehicle charging station.

Power transformers usually work stably in harsh environments with good reliability, and with the updating of materials and structural improvements, the performance is gradually improving. In the application of power electronic transformers in medium and high power occasions, Boost PFC not only has the traditional transformer function but also has a variety of system functions, which provides a new way of thinking for solving the challenges faced by the depth of power grid intelligence. This paper introduces the basic principle and topology of Boost PFC, which has the advantages of less power conversion and higher operating efficiency. Based on the average current mode control scheme of Boost PFC, a duty cycle direct calculation control strategy without current sensor is realized by simplifying the control. This control strategy puts most of the arithmetic

[1] School of International Education, Hebei University of Technology, Tianjin 300401, Tianjin, China.Email:LHWang@163.com

work in the main program, i.e., multiple switching cycles, while only voltage sampling and duty cycle calculation are required in each interrupt program. The proposed control strategy eliminates the current sensor and reduces the control cost. Meanwhile, the direct calculation of duty cycle is used to replace the PI regulation of the current inner loop. The operation efficiency, work performance and reliability of the power electronic transformer enriched by the control strategy will be gradually improved, especially in the smart grid, energy Internet and other smart grids with a broad application prospect.

2. RELATED WORKS

High-performance power electronic converters have a wide range of applications in modern power systems and electronic devices, enabling efficient conversion and control of electrical energy and providing high-quality power supply. However, high-performance power electronic converters face severe thermal design challenges as the power density continues to increase and the operating frequency increases.Saafan, A. A et al. present a novel multiport DC-DC converter designed for DC microgrids. The converter optimizes microgrid performance by reducing the number of power conversions, component count and providing boost capability. Its bidirectional buck-boost structure enhances the flexibility of connecting sources/loads with different voltages and power levels. The control strategy realizes PV MPPT and DC power resilience to ensure stable control of DC link voltage. Steady-state analysis reveals the inter-port voltage relationship, and small-signal modeling and control design further enhance the performance.MATLAB/Simulink simulations and experiments validate the efficient and reliable performance of the converter under different conditions [8]. Fu, X et al. investigated the stability of a three-phase voltage-sourced converter under grid-connected and grid-tracking control. By constructing an energy function model, the differences between the two control strategies were compared and the effects of system parameters on stability were analyzed. It is found that the grid tracking control exhibits different damping characteristics under different grid strengths, which affect the stability. Equivalent damping coefficients are proposed as a basis for selecting the control strategy for weak/strong grid conditions. Simulations and experiments verify the applicability of the control strategy under different grid strengths and provide theoretical guidance for the stability control of the grid-connected system [9]. Abdel-Rahim, O et al. proposed high boost DC/DC converter with MPC-MPPT algorithm based on the optimal number of sensors to reduce the system cost. The converter provides high voltage gain and MPC technique ensures excellent performance. The dual sensor MPPT technique is validated effective in different scenarios and simulation and experimental results are consistent, proving that the system is efficient and stable [10]. Tayyebi, A et al. explore the importance of grid formation strategies in low inertia power systems and analyze the impact of grid-connected converters on the frequency stability of the system through a case study that points out the link between the DC dynamics and the AC current limitation. The interaction between fast GFC and slow SM is investigated to reveal its impact on system stability and to provide guidance for the control design of low-inertia systems [11]. Rafi, M. A. H et al. comprehensively reviewed DCFC station with energy storage, explored its motivation, architecture, power electronic converter technology, and analyzed the performance under different charging scenarios through simulation. The study not only focuses on the academic frontiers, but also covers the applications of actual energy storage projects worldwide, providing a reference for the optimization of DCFC stations [12]. Zhang, Q et al. proposed a Laplace transform-based DSC IIG short-circuit analytical model, which takes into account the controller delays, parameters, and LV ride-through strategies, providing theoretical support for realistic protection settings. Simulations and experiments verified the validity and applicability of the model [13]. Noël, P et al. faced with the dual challenge of increasing power consumption in electronics and communication systems, explored the potential of non-traditional materials and state variables in reducing power consumption. A new method based on strontium titanate ferroelectric states to modulate the spin-orbit

properties of two-dimensional electron gases was proposed to achieve low-power spin detection, opening new avenues for the development of ultra-low-power spintronics [14]. Salem, A et al. reviewed the recent advances in multilevel inverters, MLIs, in particular those novel topologies aiming to reduce the number of components.MLIs are characterized by their waveform quality, modular design, transformerless operation, etc. are favored in energy conversion systems, but high cost is its main challenge. The primary objective of the article is to summarize and analyze the advantages, disadvantages, structures, and applications of the latest low-component-count MLI topologies. Secondly, a new comparative approach considering component ratings is innovatively proposed to evaluate different topologies more comprehensively. The effectiveness of the new methodology is verified through a detailed comparative study, which provides new perspectives and tools for MLI design [15].

3. TOPOLOGY OF HIGH-PERFORMANCE POWER ELECTRONIC CONVERTERS

3.1 Principle of operation of the converter

Most of the electrical equipment, the power supply often comes directly from the AC power grid, but almost all commonly used electronic circuits must be used in the DC power supply mode, so the AC / DC converter has become an indispensable part of the electronic products. The use of diode rectifier, capacitor filter rectifier link to obtain DC power supply often makes the input current serious distortion, not only on the power supply to produce serious electromagnetic interference, so that the power factor decreases, and can not meet the complex precision instruments and equipment on the stability of the power supply and other aspects of the higher requirements [16-17]. Therefore, the study of high power factor and low output ripple PFC converter is of great significance, power electronic transformer types, but mainly by the power electronic devices constitute the primary and secondary power electronic converter, connecting the high frequency transformer constitutes the power transmission equipment, the converter principle of operation as shown in Figure 1. The high-voltage side of the industrial frequency alternating current modulation into high-frequency alternating current, through the high-frequency transformer coupling to generate an induced electromotive force, by the secondary converter will be high-frequency alternating current modulation into industrial frequency alternating current, so as to supply power to the load [18]. The voltage ratio of the converter is the amplitude ratio of the AC input voltage to the AC output voltage, so smooth regulation can be achieved by simply changing the ratio of the high frequency transformer.

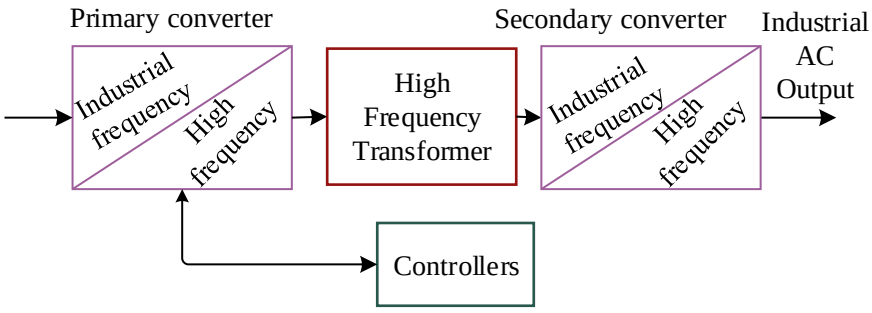

Figure 1 Principle of operation of the converter

High-frequency transformer with voltage level change, electrical isolation and other functions, small size and light weight, its transformer capacity as shown in formula (1):

$$S = 2.22 * K * f * J * Ac * Ae * Bm \quad (1)$$

Where, K represents the copper wire saturation factor, f represents the excitation frequency, Ac

represents the core area, Ae represents the conductor area, J represents the conductor current density, and Bm represents the maximum flux density. By determining the materials, it is possible to derive a fixed K, J, Bm, when increasing the frequency can reduce the size of the transformer.

3.2 Topology of the Dual Boost PFC

Power electronic devices have been widely used in various fields, and the harmonic pollution existing in AC and DC systems requires power factor correction. And the circuit topology and control strategy of the converter are the current popular research objects in this field [19]. Boost converter has the advantages of simple structure, stable performance of power factor correction, and low requirements on the control chip, so it becomes the most commonly used circuit in the power factor correction converter. In terms of control strategy design, the traditional PFC control method is double closed-loop PI control, which has a good control effect in the case of static system response. However, in the case of large perturbations in the system parameters, this type of control algorithm cannot satisfy the constraints of its own parameters well, because this type of control strategy is based on the constant parameters of the system, ignoring several nonlinear factors in the mathematical modeling of the system. Therefore these factors cause the system to lose performance and produce poor control results when the parameters are varied [20].

For this reason, many more nonlinear control algorithms have been born in the design of control strategies. Although these methods can maintain good dynamic characteristics when the system generates large disturbances, these control algorithms all have the same drawback, i.e., when the load disturbance is large, the dynamic adjustment of the system takes a long time, resulting in poor robustness [21]. At the same time, these control laws are more complex in design and have higher requirements for the processor in hardware debugging.Boost as the most widely used topology in power factor correction converters, the dual Boost PFC converter is shown in Fig. 2. A dual Boost PFC converter usually consists of two Boost PFC converters connected in parallel to achieve higher power density and better performance. SCR_1 and SCR_2 act as thyristors for current control. AC represents the alternating current, while L_1 and L_2 act as inductors for further current handling. T_1 and T_2 act as two switching tubes. In Boost PFC converter, switching tubes are one of the core components which are used to control the charging and discharging process of the inductor to control the output voltage and input current. D_1 and D_2 act as the continuity diodes to provide a continuity path for the current in the inductor when the switching tubes are turned off.

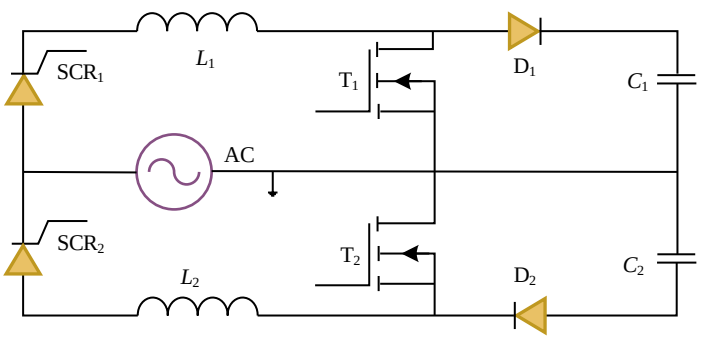

Figure 2 Dual Boost PFC converter

Boost PFC converter equivalent circuit shown in Figure 3, Figure 3(a) for the utility operates in the positive half-cycle, SCR_1 turn on, L_1, T_1, D_1 Boost PFC circuit composed of positive bus voltage. Figure 3(b) the utility operates in the negative half-cycle, SCR_2 open L_2, T_2, D_2 Boost PFC circuit composed of negative bus voltage.

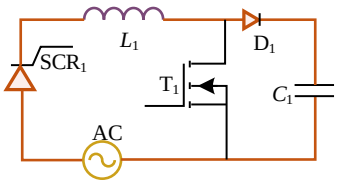

(a) Utility positive half-wave equivalent circuit

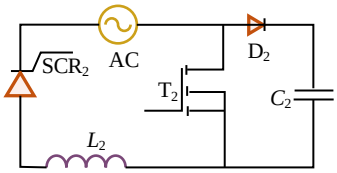

(b) Utility negative half-wave equivalent circuit

Figure 3 Equivalent circuit for dual Boost PFC operation

Double Boost PFC converter in the utility power positive, negative half cycle respectively, the formation of positive and negative bus voltage is relatively independent, through the analysis of the basic principle of operation can be seen that its positive and negative bus voltage ripple is equivalent to the Boost PFC bus voltage secondary ripple were transferred to the positive and negative bus. Research Boost PFC converter work secondary ripple change rule, can get double Boost PFC bus voltage secondary ripple change rule.

4. INTELLIGENT CONTROL STRATEGY DESIGN

4.1 CCM control method

Fixed-load Boost PFC converters select the mode of operation of the inductor current and design the inductors according to the output power.Boost PFC converters operate in discontinuous conduction mode over the entire power range and are usually suitable for low power applications. In medium and high power applications, the converter inductor parameters are usually designed based on continuous conduction mode conditions [22]. However, the output power must reach a certain value to satisfy the operating conditions in continuous conduction mode. As the load decreases or the input voltage increases, the input current decreases. At this time, the inductor will not be able to continue to work in continuous conduction mode and it will work in intermittent conduction mode for a certain time and continuous conduction mode for a certain time, i.e., continuous conduction mode (CCM) is proposed in this paper.

Assuming that the starting moment of the n st switching cycle is $t(n-1)$ and the ending moment is $t(n)$ and the duty cycle is $d(n)$, let $d'(n)=1-d(n)$. Due to f_s □ f, therefore, the visible input voltage uin is constant during a switching cycle T_s. For the n th T_s, the analysis is carried out to obtain:

$$d^{'}(n)=\frac{\left|U_{in}(n)\right|-Ldi_{L}/dt}{U_{o}(n)},t(n-1)\le t\prec t(n) \tag{2}$$

Since $i_L=\left|i_{in}\right|=I_{mp}\left|\sin\omega t\right|$, I_{mp} denote the peak input current, then equation (2) can be written as:

$$d^{'}(n)=\frac{\left|U_{in}(n)\right|-L\left(\left|i_{in}(n)\right|-\left|i_{in}(n-1)\right|\right)/T_{s}}{U_{o}(n)} \tag{3}$$

When the Boost circuit realizes PFC, the input current $i_{in}(n)$ must track the reference current $i_{ref}(n)$. At the same time, the output voltage U_o should track the reference voltage u_{ref}. The sampling coefficients of the circuit parameters $K_dU_o(n)=u_{ref}$. Are still the same as in the case of the double-loop control although the current at the inputs is not sampled assuming that $K_d\left|i_{in}(n)\right|=i_{ref}(n)$, $K_d\left|i_{in}(n-1)\right|=i_{ref}(n-1)$, and by substituting these three relationships into Eq. (3), it can be derived:

$$d^{'}(n)=\frac{K_d\left|U_{in}(n)\right|-L\left(\left|i_{ref}(n)\right|-\left|i_{ref}(n-1)\right|\right)/T_{s}}{U_{ref}} \tag{4}$$

where $i_{ref}(n)=I_{mp}\sin\left[\omega t(n)\right]$, satisfying equation (3) realizes the PFC of the circuit. I_m as the amplitude of i_{ref} is determined by the output signal of the voltage loop. By sampling the input rectified voltage $u(n)$ in the program, its half-wave average is first calculated and then converted to the amplitude $u_{in}(n)$, according to $\sin\left[\omega t(n)\right]=u_{in}(n)/U_{mp}=K_du_{in}(n)/K_dU_{mp}$, $\sin\left[\omega t(n)\right]$ can be obtained.

4.2 Duty Cycle Analysis

Due to $d(n)=1-d^{'}(n)$, let $d(n)=d_1(n)+d_2(n)$, the expression is derived through Eq. (4) as:

$$d(n)=d_1(n)+d_2(n)=\frac{u_{ref}-K_d\left|u_{in}(n)\right|}{u_{ref}}+\frac{L\left(\left|i_{ref}(n)\right|-\left|i_{ref}(n-1)\right|\right)/T_{s}}{u_{ref}} \tag{5}$$

The first item $d_1(n)$ is determined by feedback u_{in}, which compensates to some extent for the effect of changes in u_{in} on U_o and ensures that when u_{in} fluctuations occur, U_o can adjust quickly and remain essentially stable.

The second term $d_2(n)$ is given by i_{ref} and consists of the voltage loop output and the unit sinusoidal value, ensuring that $i_{in}(n)$ is able to track $i_{ref}(n)$.

The advantages of this algorithm over the average current control scheme are as follows:
(1) There is no need to sample the coil current, which saves the current sensor and reduces the control cost [23].
(2) Direct duty cycle calculation is used instead of the current inner loop calculation. This algorithm is simpler, reduces the amount of calculation, saves DSP resources, and improves f_s.

(3) The traditional PI control is a process of gradually eliminating the error, and the control speed is slow. The algorithm is based on the constraint relationship and directly calculates the duty cycle required to reach the i_{ref} inductor current at the end of the switching cycle, which can improve the regulation speed.

4.3 Voltage control loop

In steady state, according to the basic relationship between diode current and inductor current in Boost converter:

$$i_{VD} = d^{'} i_L = d^{'} \left| i_{ref} \right| = d^{'} I_{mp} \left| \sin \omega t \right| \tag{6}$$

By substituting equation (4) into equation (6), the average value of the diode current over half a cycle of the supply voltage is calculated. Since u_{in} and i_{ref} are proportional, when the circuit realizes PFC, the resulting equation is:

$$I_{VD} = \frac{K_d U_{mp} I_{mp}}{2U_{ref}} = \frac{U_{mp} I_{mp}}{2U_o} = \frac{\xi I_m^2}{2U_o} \tag{7}$$

There is a slow equivalent scaling factor ξ in Eq. Small signal perturbation according to Eq. (7) is performed by neglecting the product term of the small signal components and removing the DC term to obtain the small signal expression:

$$\xi I_m \tilde{I}_m = \tilde{U}_o I_{VD} + U_o \tilde{I}_{VD} \tag{8}$$

When Boost is connected to a constant power load, the small signal is represented as:

$$\tilde{I}_{VD} = C \frac{d\tilde{U}_o}{dt} - \frac{I_o}{U_o} \tilde{U}_o \tag{9}$$

Substituting Eq. (9) into Eq. (8) and considering that the average current flowing through the diode is equal to the load current, the transfer function of the voltage loop can be obtained [24]. The Laplace transform of the transfer function is：

$$G_u(s) \frac{\tilde{U}_o(s)}{\tilde{I}_m(s)} = \frac{\xi I_m}{sCU_o K_d^2} \tag{10}$$

The voltage loop gain $T_u = K_d G_{PI} G_u(s)$, at the voltage loop crossover frequency f_{cu}, the loop gain is 1. The compensator gain can be calculated as:

$$G_{PI} = \left| \frac{2\pi f C U_o K_d}{\xi I_m} \right|_{f = f_{cu}} \tag{11}$$

Assuming the zero of the compensator is at f_{cu}, the integration time constant of the PI controller is $T = 1/(2\pi f_{cu})$ such that the transfer function of the PI controller can be found.

5. ELECTRONIC CONVERTER TOPOLOGY AND CONTROL ANALYSIS

5.1 Inputs and outputs

In this paper, PSIM software is used to build a simulation circuit to simulate and analyze the circuit and control parameters designed in the previous section, and verify the correctness of the circuit design. Figure 4 shows the input voltage and data current waveforms, 220V single-phase AC input, DC output voltage is 336V, the output power is 3.6kW, and the load carried is a fixed power load. From the simulation waveforms, the input current tracks the waveform of the input voltage in phase and maintains a good sinusoidal characteristic, and the power factor of the input reaches more than 0.9.

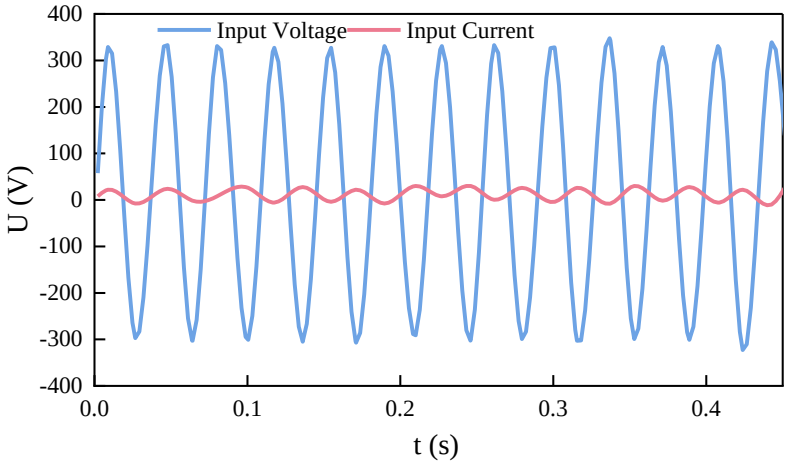

Figure 4 Input voltage and data current waveforms

Fig. 5 shows the output voltage waveform, and the output voltage is stabilized at about 336 V, which reflects good stability.

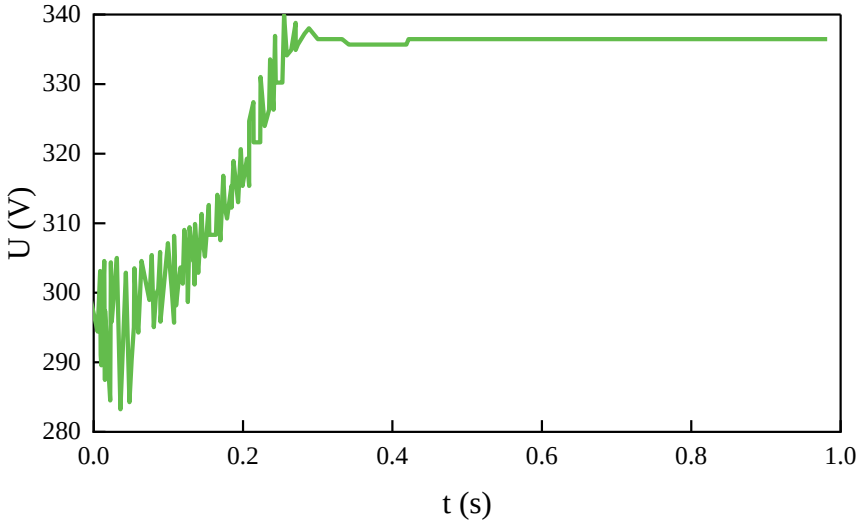

Figure 5 Output voltage waveform

5.2 Performance comparison results

5.2.1 Input Voltage and Current

Figure 6 shows the input voltage waveform and the two-phase inductor current waveform, it can be seen that the two-phase inductor current waveforms are sinusoidal half-waves, which are basically consistent in phase and amplitude, indicating that the current flowing through the two-phase inductor is basically of the same magnitude, and two-phase equalization of the current is achieved. Compared with the input voltage waveform, the inductor current waveform can track the phase of the input voltage waveform well, and it fluctuates around -270V and -210V between 0-200ms, which indicates that the input current can track the phase of the input voltage well at the AC input.

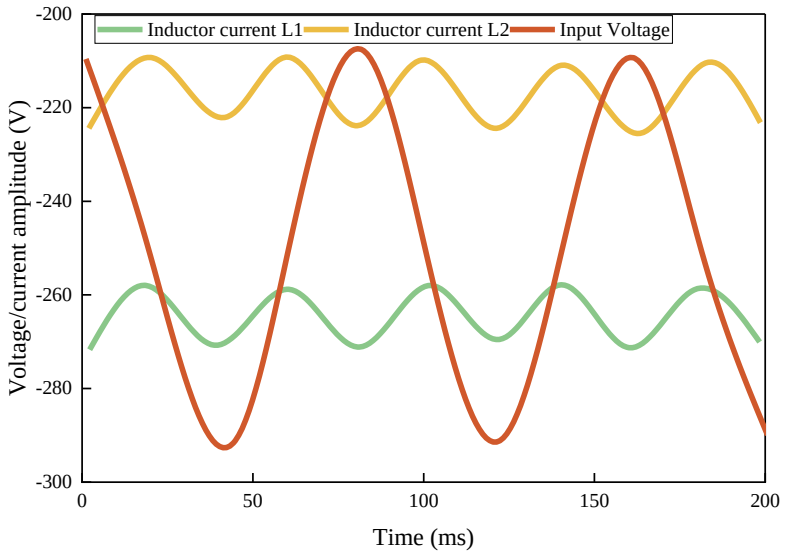

Figure 6 Input voltage waveforms and inductor current waveforms

Fig. 7 shows the input voltage waveform and the input current waveform, which shows that the input current has good sinusoidal characteristics, and the phase is basically the same as the phase of the input voltage at 1.5ms and 2.5ms. After 4.2ms, the amplitude of the input current is about twice the amplitude of the inductor current in each phase, indicating that the circuit is able to adjust its output power according to the change of the input current to meet different load demands.

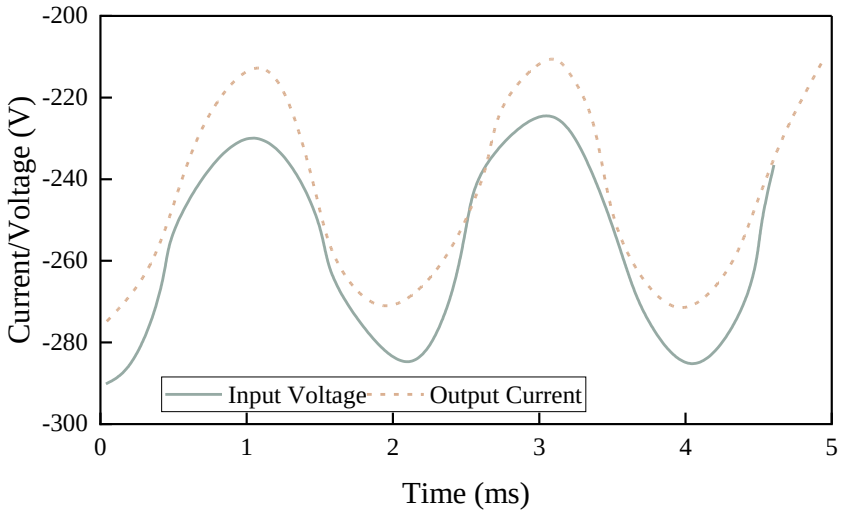

Figure 7 Input voltage waveforms and input current waveforms

Then the parameter variables of the control algorithm designed in this paper are simulated in different system states, and the waveforms of each parameter variable in the simulation circuit are shown in Fig. 8. Fig. 8(a) shows the steady state of the system, the starting load is under the condition of 200 Ω. The input current is able to track the input voltage accurately under this control strategy, which presents a good power factor correction characteristic. The output voltage is stabilized at the desired voltage setting value of 200 V. From the whole process of startup to stabilization, it is seen that the system responds to the regulation in 4 ms and there is no obvious overshooting phenomenon. Compared with the traditional control method, the control algorithm has a faster response time and good steady-state response characteristics.

Figure 8(b) shows the system perturbation, when the load is changed abruptly from 200Ω to 100Ω, the input current still tracks the input voltage accurately, the output voltage maintains the constant voltage setting value of 230V, and the output voltage is not affected by the DC component in any way except for the ripple which is slightly increased, so it has a good dynamic response characteristic.

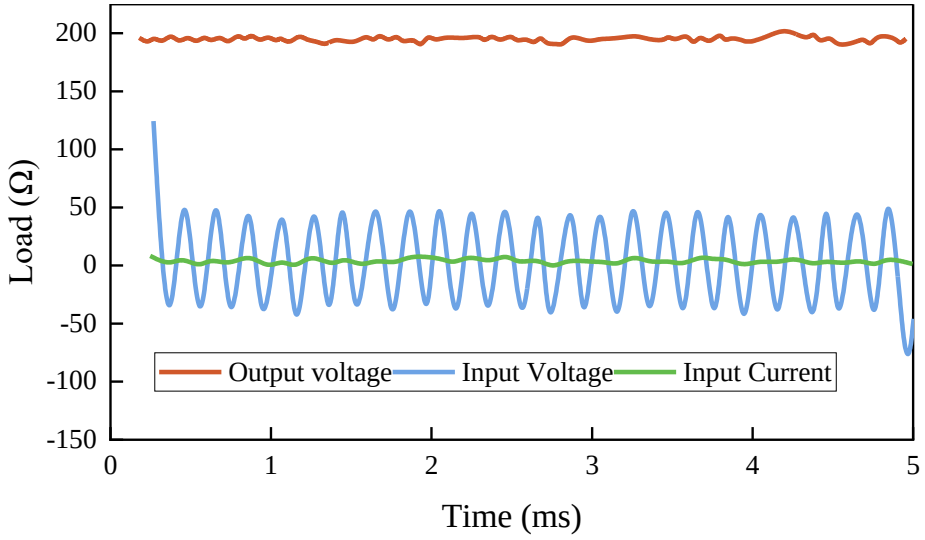

(a) System steady state

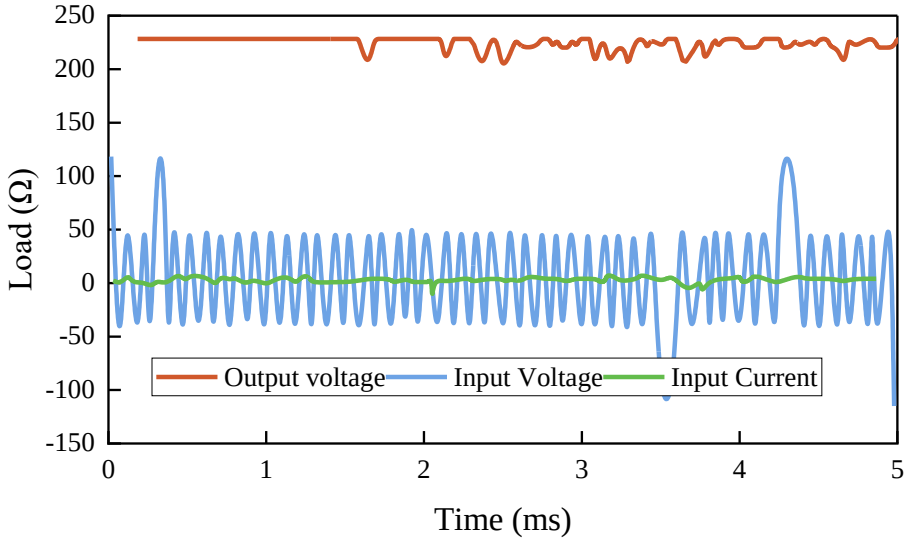

(b) System perturbation

Figure 8 Simulated waveforms for each parameter

5.2.2 Input-output efficiency

The efficiency of the circuit is analyzed at an input voltage of 230 V. At light load, the overall efficiency of the

circuit is low, and the output power is gradually increased with the decrease of the load resistance value, and the output efficiency remains stable at nearly full load. The results of the current efficiency analysis are shown in Table 1. It can be seen that as the input current increases from 1.50 A to 9.45 A, the output current also increases accordingly from 0.60 A to 5.95 A. This shows that the circuit is able to adjust its output power according to the changes in input current to meet different load demands. The output voltage remained around 336.0 V for most of the experiments, with only a slight increase of 336.1 V in the fourth experiment.This small fluctuation was caused by measurement errors or small changes in the circuit, but overall the output voltage was stable. At a low input current of 1.50A, the efficiency is relatively low at 0.58%, which is due to the high efficiency loss of the circuit under light load condition. As the input current increases, the efficiency gradually increases and reaches a maximum value of 0.93% at an input current of 6.08A. This shows that the circuit has high efficiency at medium load. However, when the input current is further increased such as 8.51A and 9.45A, the efficiency does not continue to increase but decreases slightly remaining around 0.92. This is due to the loss of efficiency due to certain limitations of the circuit at high loads.

Table 1 Circuit efficiency analysis results

Serial number	**Serial number Input voltage/V**	**Input Current/A**	**Output Voltage/V**	**Output Current/A**	**Efficiency/%**
1	230	1.50	335.9	0.60	0.58
2	230	3.90	336.0	2.08	0.78
3	230	4.78	336.0	2.98	0.91
4	230	6.08	336.1	3.87	0.93
5	230	8.51	336.0	5.36	0.92
6	230	9.45	336.0	5.95	0.92

Overall, the efficiency of the circuit performs well, especially at moderate loads. However, there is still room for efficiency improvement under light and high loads. For practical applications, it is important to understand the efficiency performance of the circuit under different loads in order to select appropriate operating conditions and optimize the circuit design to improve efficiency.

In order to realize the effective control of high-performance power electronic converters. The CCM control strategy of this paper is compared and analyzed with the MPPT control strategy and the MPC-MPPT control strategy, and the performance of the different strategies is shown in Table 2.The CCM mode shows a faster regulation speed in this case, and it takes only 30ms to reach the new steady state, and the voltage variation is only 1V, which indicates that it has a good stability and a faster response speed. This is because the CCM regulates the voltage indirectly by directly controlling the current, which enables the system to respond quickly to changes in the voltage reference value. In contrast, the MPPT performs poorly when the voltage reference value increases suddenly. Its regulation time is up to 160ms, which is almost more than five times that of the CCM, indicating that the system response is slower. In addition, the voltage variation is also larger by 4.5 V, indicating that the voltage fluctuates more during the regulation process, and the stability is not as good as that of the CCM.The performance of the MPC-MPPT in the sudden increase of the voltage reference value is between that of the CCM and the MPPT. Its regulation time is 90ms, which is slower than CCM but much faster than MPPT. The voltage variation is 3V, which is also smaller than MPPT, indicating that the MPC algorithm improves the response speed and voltage stability of MPPT to some extent. The above analysis shows that the

CCM control strategy proposed in this paper exhibits the fastest regulation speed and the best voltage stability when the voltage reference value increases suddenly.

Table 2 Performance of different strategies

Different control strategies	**Sudden increase in voltage reference**	**Load surge**
	Adjustment time/ms	**Amount of voltage change/V**
CCM	30	1
MPPT	160	4.5
MPC-MPPT	90	3

6. CONCLUSION

In this paper, a power electronic converter with superior performance is obtained by using dual BoostPFC topology and CCM control method. Effective verification of its performance is achieved through simulation and experimental analysis of the circuit and control parameters. The conclusions are as follows:

(1) The input current can track the input voltage well, with consistent phase and good sinusoidal characteristics, and the power factor reaches above 0.9. The output voltage is stabilized at about 336 V with good stability, and the CCM control strategy shows the fastest regulation speed and the best voltage stability with the regulation time of only 30 ms and the voltage change of only 1 V when the voltage reference value increases suddenly.

(2) Under the input voltage of 230V, the circuit has a high efficiency of 0.93% at medium load, but there is still room for improvement in the efficiency at light load and high load. Compared with the MPPT and MPC-MPPT strategies, the CCM strategy has obvious advantages in terms of regulation speed and voltage stability.

In summary, the topology and control strategy proposed in this paper can meet the requirements of high-performance power electronic converters.

REFERENCES

[1] Zhang, H., Xiang, W., Lin, W., & Wen, J. (2021). Grid forming converters in renewable energy sources dominated power grid: Control strategy, stability, application, and challenges. *Journal of modern power systems and clean energy*, *9*(6), 1239-1256.

[2] Wei, Y., Luo, Q., & Mantooth, A. (2020). Overview of modulation strategies for LLC resonant converter. *IEEE Transactions on Power Electronics*, *35*(10), 10423-10443.

[3] Xu, Q., Vafamand, N., Chen, L., Dragičević, T., Xie, L., & Blaabjerg, F. (2020). Review on advanced control technologies for bidirectional DC/DC converters in DC microgrids. *IEEE Journal of Emerging and Selected Topics in Power Electronics*, *9*(2), 1205-1221.

[4] Liu, C., Chau, K. T., Lee, C. H., & Song, Z. (2020). A critical review of advanced electric machines and control strategies for electric vehicles. *Proceedings of the IEEE*, *109*(6), 1004-1028.

[5] Zhao, S., Blaabjerg, F., & Wang, H. (2020). An overview of artificial intelligence applications for power electronics. *IEEE Transactions on Power Electronics*, *36*(4), 4633-4658.

[6] Shao, S., Chen, L., Shan, Z., Gao, F., Chen, H., Sha, D., & Dragičević, T. (2021). Modeling and advanced control of dual-active-bridge DC–DC converters: A review. *IEEE Transactions on Power Electronics*, *37*(2), 1524-1547.

[7] Rodriguez, J., Garcia, C., Mora, A., Davari, S. A., Rodas, J., Valencia, D. F., ... & Mijatovic, N. (2021). Latest advances of model predictive control in electrical drives—Part II: Applications and benchmarking with classical control methods. *IEEE Transactions on Power Electronics*, *37*(5), 5047-5061.

[8] Saafan, A. A., Khadkikar, V., El Moursi, M. S., & Zeineldin, H. H. (2022). A new multiport DC-DC converter for DC microgrid applications. *IEEE Transactions on Industry Applications*, *59*(1), 601-611.

[9] Fu, X., Sun, J., Huang, M., Tian, Z., Yan, H., Iu, H. H. C., ... & Zha, X. (2020). Large-signal stability of grid-forming and grid-following controls in voltage source converter: A comparative study. *IEEE Transactions on Power Electronics*, *36*(7), 7832-7840.

[10] Abdel-Rahim, O., & Wang, H. (2020). A new high gain DC-DC converter with model-predictive-control based MPPT technique for photovoltaic systems. *CPSS Transactions on Power Electronics and Applications*, *5*(2), 191-200.

[11] Tayyebi, A., Groß, D., Anta, A., Kupzog, F., & Dörfler, F. (2020). Frequency stability of synchronous machines and grid-forming power converters. *IEEE Journal of Emerging and Selected Topics in Power Electronics*, *8*(2), 1004-1018.

[12] Rafi, M. A. H., & Bauman, J. (2020). A comprehensive review of DC fast-charging stations with energy storage: Architectures, power converters, and analysis. *IEEE Transactions on Transportation Electrification*, *7*(2), 345-368.

[13] Zhang, Q., Liu, D., Liu, Z., & Chen, Z. (2021). Fault modeling and analysis of grid-connected inverters with decoupled sequence control. *IEEE Transactions on Industrial Electronics*, *69*(6), 5782-5792.

[14] Noël, P., Trier, F., Vicente Arche, L. M., Bréhin, J., Vaz, D. C., Garcia, V., ... & Attané, J. P. (2020). Non-volatile electric control of spin–charge conversion in a SrTiO3 Rashba system. *Nature*, *580*(7804), 483-486.

[15] Salem, A., Van Khang, H., Robbersmyr, K. G., Norambuena, M., & Rodriguez, J. (2020). Voltage source multilevel inverters with reduced device count: Topological review and novel comparative factors. *IEEE transactions on power electronics*, *36*(3), 2720-2747.

[16] Benlahbib, B., Bouarroudj, N., Mekhilef, S., Abdeldjalil, D., Abdelkrim, T., & Bouchafaa, F. (2020). Experimental investigation of power management and control of a PV/wind/fuel cell/battery hybrid energy system microgrid. *International Journal of Hydrogen Energy*, *45*(53), 29110-29122.

[17] Muhtadi, A., Pandit, D., Nguyen, N., & Mitra, J. (2021). Distributed energy resources based microgrid: Review of architecture, control, and reliability. *IEEE Transactions on Industry Applications*, *57*(3), 2223-2235.

[18] Wang, L., Madawala, U. K., & Wong, M. C. (2020). A wireless vehicle-to-grid-to-home power interface with an adaptive DC link. *IEEE Journal of Emerging and Selected Topics in Power Electronics*, *9*(2), 2373-2383.

[19] Chen, M., Zhou, D., & Blaabjerg, F. (2020). Modelling, implementation, and assessment of virtual synchronous generator in power systems. *Journal of Modern Power Systems and Clean Energy*, *8*(3), 399-411.

[20] Dao, N. D., & Lee, D. C. (2020). High-efficiency hybrid LLC resonant converter for on-board chargers of plug-in electric vehicles. *IEEE Transactions on Power Electronics*, *35*(8), 8324-8334.

[21] Sun, X., Wu, M., Lei, G., Guo, Y., & Zhu, J. (2020). An improved model predictive current control for PMSM drives based on current track circle. *IEEE Transactions on Industrial Electronics*, *68*(5), 3782-3793.

[22] Wang, Z., Liu, W., He, W., Guo, H., Long, L., Xi, Y., ... & Hu, C. (2021). Ultrahigh electricity generation from low-frequency mechanical energy by efficient energy management. *Joule*, *5*(2), 441-455.

[23] Wang, C., Hua, L., Yan, H., Li, B., Tu, Y., & Wang, R. (2020). A thermal management strategy for electronic devices based on moisture sorption-desorption processes. *Joule*, *4*(2), 435-447.

[24] Sun, X., Cao, J., Lei, G., Guo, Y., & Zhu, J. (2021). A robust deadbeat predictive controller with delay compensation based on composite sliding-mode observer for PMSMs. *IEEE Transactions on Power Electronics*, *36*(9), 10742-10752.

ABOUT THE AUTHOR

Linhao Wang

School of International Education, Hebei University of Technology, Tianjin 300401, Tianjin, China

E-mail: LHWang@163.com